

Crystal Structures, Terahertz Spectra and Dye Adsorption Performance of Three Lanthanide-bisphosphonate Complexes Containing Keggin Polyoxometalates^①

WANG Zhi-Qiang^{a, b} PAN Xun^a LU Yan-Lei^a LI Ying-Yu^a
YANG Yu-Ping^c XIN Xiu-Lan^a JIN Qiong-Hua^{a, b②}

^a (Department of Chemistry, Capital Normal University, Beijing 100048, China)

^b (State Key Laboratory of Structural Chemistry, Fujian Institute of Research on the Structure of Matter, Chinese Academy of Sciences, Fuzhou 350002, China)

^c (School of Science, Minzu University of China, Beijing 100081, China)

ABSTRACT Three lanthanide complexes [LnL₃(H₂O)]PMo₁₂O₄₀·CH₃CN (Ln = Dy³⁺ for **1**, Ln = Ho³⁺ for **2**, Ln = Lu³⁺ for **3**, L = tetraethyl ethylenediphosphonate) have been synthesized, and characterized by single-crystal X-ray diffraction, elemental analysis, IR, PXRD, thermogravimetric analysis and terahertz time-domain spectroscopy (THz-TDS). Structural analysis results show that they have the same coordination mode and similar steric structures. Complexes **1**~**3** all crystallize in the monoclinic crystal system with space group *P*2₁/*c*. The centered Ln(III) obtained a seven-coordinated mononuclear structure by linking with three tetraethyl ethylenediphosphonates and one water molecule, resulting in a three-dimensional supramolecular structure through hydrogen bonding. The three complexes have good adsorption properties for rhodamine B (RhB) in powder state. Moreover, terahertz time-domain spectroscopy (THz-TDS) was applied to represent the structures of complexes and ligands, which will provide useful information for establishing bridge between THz and complex structure in coordination chemistry.

Keywords: lanthanide complexes, POMS, tetraethyl ethylenediphosphonate, structure, terahertz time-domain spectroscopy (THz-TDS); DOI: 10.14102/j.cnki.0254-5861.2011-2987

1 INTRODUCTION

In recent years, lanthanide complexes have been extensively studied and reported in terms of luminescence^[1-3], catalysis^[4-6] and magnetism^[7-9]. As an important area in the coordination chemistry of lanthanide metals, complexes with phosphine oxides have attracted much attention^[10]. Anna G. Matveeva group have ever reported a series of lanthanide complexes by using hybrid scorpionate (OPPh₂)₂CHCH₂C(O)Me as ligand, and the coordination modes vary with the polyhedron of metals and the nature of solvent^[11]. Phosphonate has similar characteristics and properties to phosphine oxide groups (P=O), and corresponding complexes usually exhibit excellent properties and potential applications while rare work was carried out on

lanthanide^[12-14]. In terms of hard acid, the lanthanide metal cation has very strong oxygen affinity and can easily interact with highly polar oxygen-containing groups to form a variety of complexes and coordination polymers. In this paper, following the Hard-Soft-Acid-Base (HSAB) theory, tetraethyl ethylenediphosphonate was adopted to coordinate with lanthanide ions. The ratio of Ln:L = 1:3, and the ligand chelating with the central ion satisfies the high coordination number of lanthanide ions. The mixed solvent of acetonitrile and water was found more conducive to the formation of high-quality, high-yield crystals. Besides, polyoxometalates (POMs) functionalized materials have broad application prospects in magnetic materials, catalysis, energy conversion and energy storage materials^[15-17]. So, POM-based organic-inorganic hybrids complexes have been an attractive topic^[18, 19].

Received 21 September 2020; accepted 25 February 2021 (CCDC 2008545 for **1**, CCDC 2008546 for **2** and CCDC 2008544 for **3**)

① This work was supported by the National Natural Science Foundation of China (Nos. 21171119 and 11574408) and the Beijing Municipal Natural Science Foundation (Nos. 2172017 and 2172012)

② Corresponding author. E-mail: jinqh@cnu.edu.cn

In this work, the Keggin-type $[\text{PMo}_{12}\text{O}_{40}]^{3-}$ was added to the system without coordinating with $\text{Ln}(\text{III})$ but exists as an anion. According to Platon calculation and crystal structure analysis, there are hydrogen bonds between $[\text{PMo}_{12}\text{O}_{40}]^{3-}$ anions and phosphonate, and $[\text{PMo}_{12}\text{O}_{40}]^{3-}$ acts as a template in the entire complex structure.

In addition, the terahertz time-domain spectra (THz-TDs) of the composite material at $0.2\sim 2.8$ THz ($6.6\sim 92.4$ cm^{-1}) were measured at room temperature. This technique has been proven to detect free electron motion, molecular rotation modes, lattice vibration and dipole transitions, which can characterize the way of intermolecular interactions^[20-22]. According to our previous work, we have synthesized a number of lanthanide complexes with the bisphosphonate ligand and characterized them by terahertz time-domain spectroscopy^[23-25]. Herein, we first adopt THz-TDS to characterize lanthanide-bisphosphonate complexes based on POMs modification.

2 EXPERIMENTAL

2.1 Materials and measurements

All commercially available initial reagents were used without furthermore treatment. FT-IR spectra (KBr pellets) were measured on a Perkin-Elmer Infrared spectrometer. C, H and N elemental analyses were carried out on an Elementar Vario MICRO CUBE (Germany) elemental analyzer. UV-Vis spectra were gained from a 2550 UV-Vis spectrophotometer (Shimadzu, Japan). The THz absorption spectra were recorded on a THz time domain device of Minzu University of China and carried out in a N_2 atmosphere to avoid the influence of water vapor, based on photoconductive switches for the generation and electro-optical crystal detection of the far-infrared light, effective frequency in the range of $0.2\sim 2.8$ THz.

2.2 Syntheses of the complexes 1~3

A mixture of 0.2 mmol $\text{Ln}(\text{NO}_3)_3 \cdot 6\text{H}_2\text{O}$ (Dy for **1**, Ho for **2**, Lu for **3**), $\text{H}_3\text{PMo}_{12}\text{O}_{40} \cdot n\text{H}_2\text{O}$ (0.3651 g) and L (0.1813 g, 0.6 mmol) was dissolved in the mixed solvents of 8 mL CH_3CN and 2 mL H_2O , followed by stirring for 3 hours in an 80°C water bath. The solution was filtered. Block-shaped crystals

were obtained from the filtrate after standing at room temperature for several days. The crystals of complexes **1** and **3** were yellow and that of **2** was orange.

[DyL₃(H₂O)]PMo₁₂O₄₀ · C₂H₃N (1**)** Yield: 60.19%.
Element analysis calcd. for $\text{C}_{32}\text{H}_{76}\text{DyMo}_{12}\text{NO}_{59}\text{P}_7$ (%): C, 13.03; H, 2.60; N, 0.48. Found (%): C, 13.51; H, 2.52; N, 0.56.
IR data (cm^{-1} , KBr pellets): 3469m, 2985m, 2926w, 1617w, 1476m, 1442m, 1395m, 1370w, 1304m, 1208s, 1162s, 1033s, 959s, 879s, 792s, 503s.

[HoL₃(H₂O)]PMo₁₂O₄₀ · C₂H₃N (2**)** Yield: 63.67%.
Element analysis calcd. for $\text{C}_{32}\text{H}_{74}\text{HoMo}_{12}\text{NO}_{59}\text{P}_7$ (%): C, 13.03; H, 2.53; N, 0.48. Found (%): C, 13.47; H, 2.44; N, 0.56.
IR data (cm^{-1} , KBr pellets): 3469w, 2985w, 1637w, 1476w, 1442w, 1395w, 1371w, 1304w, 1209s, 1162m, 1063s, 1033s, 958s, 880s, 803s, 503m.

[LuL₃(H₂O)]PMo₁₂O₄₀ · C₂H₃N (3**)** Yield: 55.52%.
Element analysis Calcd. for $\text{C}_{32}\text{H}_{75}\text{LuMo}_{12}\text{NO}_{59}\text{P}_7$ (%): C, 12.98; H, 2.55; N, 0.48. Found (%): C, 13.57; H, 2.29; N, 0.55.
IR data (cm^{-1} , KBr pellets): 3449w, 2985w, 1637w, 1467w, 1442w, 1396w, 1304w, 1211s, 1162m, 1063s, 1034s, 958s, 879s, 803s, 503w.

2.3 Structure determination

Single crystals of the title complexes were mounted on a Bruker Smart 1000 CCD diffractometer equipped with a graphite-monochromated $\text{MoK}\alpha$ ($\lambda = 0.071073$ nm) radiation at 298 K. Semi-empirical absorption corrections were applied using SADABS programs. All structures were solved by direct methods using SHELXS program of the SHELXTL-97 package and refined with SHELXL-97^[26, 27]. Metal atom centers were located from E-maps and other non-hydrogen atoms were located in successive difference Fourier syntheses. The final refinements were performed by full-matrix least-squares methods with anisotropic thermal parameters for non-hydrogen atoms on F^2 . The hydrogen atoms were generated geometrically and refined with displacement parameters riding on the concerned atoms.

Crystallographic data and experimental details for structural analysis are summarized in Table 1, and selected bond lengths and bond angles of complexes **1~3** are summarized in Table 2.

Table 1. Crystallographic Data for Complexes 1~3

Complex	1	2	3
Formula	$\text{C}_{32}\text{H}_{76}\text{DyMo}_{12}\text{NO}_{59}\text{P}_7$	$\text{C}_{32}\text{H}_{74}\text{HoMo}_{12}\text{NO}_{59}\text{P}_7$	$\text{C}_{32}\text{H}_{75}\text{LuMo}_{12}\text{NO}_{59}\text{P}_7$
Formula weight	2949.51	2949.92	2960.970

To be continued

<i>T</i> /K	298(2)	298(2)	293(2)
Crystal system	Monoclinic	Monoclinic	Monoclinic
Space group	<i>P</i> 2 ₁ / <i>c</i>	<i>P</i> 2 ₁ / <i>c</i>	<i>P</i> 2 ₁ / <i>c</i>
Crystal size/mm	0.20 × 0.20 × 0.20	0.20 × 0.20 × 0.20	0.20 × 0.20 × 0.20
<i>a</i> (Å)	25.628(3)	25.633(2)	25.3493(3)
<i>b</i> (Å)	14.5396(14)	14.5341(15)	14.4082(1)
<i>c</i> (Å)	24.399(2)	24.391(2)	24.0864(3)
α (°)	90.00	90.00	90
β (°)	113.534(3)	113.456(2)	113.564(1)
γ (°)	90.00	90.00	90
<i>V</i> (Å ³)	8335.2(14)	8335.9(14)	8063.69(16)
<i>Z</i>	4	4	4
<i>F</i> (000)	5688	5684.0	5704.0
Goodness-of-fit on <i>F</i> ²	1.096	1.077	1.076
<i>R</i> _{int}	0.0891	0.0834	0.2238
<i>R</i> (<i>I</i> > 2σ(<i>I</i>)) ^a	0.0779	0.0674	0.1486
<i>wR</i> (<i>I</i> > 2σ(<i>I</i>)) ^b	0.1888	0.1575	0.3069
<i>R</i> (all data) ^a	0.1523	0.1338	0.1587
<i>wR</i> (all data) ^b	0.2231	0.1835	0.3156

$$^a R = \sum (|F_o| - |F_c|) / \sum |F_o|, ^b wR = [\sum w(|F_o|^2 - |F_c|^2)^2 / \sum w(F_o^2)]^{1/2}$$

Table 2. Selected Bond Distances (Å) and Bond Angles (°) for Complexes 1~3

Complex 1					
Dy(1)–O(45)	2.293(11)	Dy(1)–O(48)	2.279(12)	Dy(1)–O(51)	2.268(12)
Dy(1)–O(54)	2.300(11)	Dy(1)–O(57)	2.295(11)	Dy(1)–O(60)	2.261(12)
Dy(1)–O(63)	2.396(13)				
O(48)–Dy(1)–O(45)	77.1(4)	O(51)–Dy(1)–O(54)	75.2(4)	O(60)–Dy(1)–O(57)	78.7(5)
Complex 2					
Ho(1)–O(60)	2.240(10)	Ho(1)–O(54)	2.264(10)	Ho(1)–O(57)	2.272(10)
Ho(1)–O(48)	2.278(10)	Ho(1)–O(51)	2.279(10)	Ho(1)–O(45)	2.281(9)
Ho(1)–O(63)	2.428(10)				
O(48)–Ho(1)–O(45)	77.3(4)	O(54)–Ho(1)–O(51)	76.3(4)	O(60)–Ho(1)–O(57)	78.1(4)
Complex 3					
Lu(1)–O(1)	2.199(16)	Lu(1)–O(3)	2.253(18)	Lu(1)–O(4)	2.184(18)
Lu(1)–O(5)	2.366(17)	Lu(1)–O(7)	2.204(18)	Lu(1)–O(9)	2.236(19)
Lu(1)–O(13)	2.259(17)				
O(1)–Lu(1)–O(13)	76.0(6)	O(4)–Lu(1)–O(3)	79.4(7)	O(7)–Lu(1)–O(9)	79.0(7)

Table 3. Intermolecular Hydrogen Bonds in Complexes 1~3

Complex 1					
Donor–H···acceptor	D–H (Å)	H···A (Å)	D···A (Å)	D–H···A (°)	Symmetry code
O(63)–H(63C)···O(13)	0.85	2.08	2.906(19)	165	
O(63)–H(63D)···N(1)	0.85	2.02	2.85(3)	165	<i>x</i> , 1+ <i>y</i> , <i>z</i>
C(3)–H(3A)···O(37)	0.97	2.51	3.26(3)	134	2– <i>x</i> , 1/2+ <i>y</i> , 3/2– <i>z</i>
C(4)–H(4C)···O(43)	0.96	2.59	3.43(3)	148	2– <i>x</i> , 1– <i>y</i> , 2– <i>z</i>
C(10)–H(10B)···O(18)	0.96	2.60	3.49(3)	155	1– <i>x</i> , 1– <i>y</i> , 1– <i>z</i>
C(12)–H(12B)···O(42)	0.97	2.54	3.41(2)	160	1– <i>x</i> , 1/2+ <i>y</i> , 3/2– <i>z</i>
C(12)–H(12B)···O(46)	0.97	2.60	3.32(2)	138	
C(24)–H(24A)···O(17)	0.96	2.37	3.25(4)	152	<i>x</i> , 1+ <i>y</i> , <i>z</i>
C(27)–H(27A)···O(17)	0.97	2.49	3.43(4)	174	<i>x</i> , 3/2– <i>y</i> , 1/2+ <i>z</i>
C(28)–H(28C)···O(9)	0.96	2.53	3.33(4)	141	<i>x</i> , 1+ <i>y</i> , <i>z</i>

To be continued

Complex 2					
Donor-H ... acceptor	D-H (Å)	H ... A (Å)	D ... A (Å)	D-H ... A (°)	Symmetric code
C(4)-H(4C) ... O(43)	0.96	2.56	3.42(3)	150	2-x, 1-y, 2-z
C(10)-H(10B) ... O(18)	0.96	2.59	3.54(3)	171	1-x, 1-y, 1-z
C(12)-H(12A) ... O(22)	0.97	2.50	3.43(2)	160	1-x, 1/2+y, 3/2-z
C(12)-H(12B) ... O(42)	0.97	2.52	3.320(19)	140	
C(19)-H(19B) ... O(9)	0.97	2.60	3.53(3)	161	
C(23)-H(23B) ... O(44)	0.97	2.57	3.53(3)	170	x, 3/2-y, -1/2+z
C(24)-H(24B) ... O(42)	0.96	2.42	3.37(3)	169	x, 3/2-y, -1/2+z
C(27)-H(27A) ... O(17)	0.97	2.46	3.43(3)	177	x, 3/2-y, 1/2+z
C(32)-H(32C) ... O(19)	0.96	2.53	3.44(2)	159	1-x, -y, 1-z
Complex 3					
Donor-H ... acceptor	D-H (Å)	H ... A (Å)	D ... A (Å)	D-H ... A (°)	Symmetric code
C(2)-H(2A) ... O(16)	0.97	2.44	3.27(4)	144	
C(3)-H(3A) ... O(28)	0.96	2.43	3.36(4)	161	x, 1/2-y, -1/2+z
C(3)-H(3B) ... O(23)	0.98	2.43	3.23(4)	138	
C(5)-H(5B) ... O(6)	0.97	2.60	3.41(5)	141	
C(9)-H(9A) ... O(12)	0.97	2.59	3.47(5)	151	1-x, 1/2+y, 1/2-z
C(12)-H(12B) ... O(11)	0.97	2.35	3.26(4)	155	x, 1/2-y, 1/2+z
C(15)-H(15A) ... O(8)	0.96	2.58	3.47(5)	155	
C(17)-H(17B) ... O(42)	0.97	2.52	3.27(5)	134	x, 1+y, z
C(19)-H(19A) ... O(34)	0.97	2.54	3.50(5)	173	x, 1/2-y, -1/2+z
C(19)-H(19B) ... O(45)	0.98	2.59	3.28(5)	127	2-x, 1-y, 1-z
C(25)-H(25B) ... O(42)	0.96	2.40	3.31(5)	158	

2.4 Dye adsorption experiment

Rhodamine B aqueous solution was used as a wastewater simulation system to study the adsorption activity of this series of complexes. The dye powder was dissolved in distilled water to obtain a 20 mg/L solution. In a typical adsorption reaction, 50 mL of 20 mg/L dye solution was stirred with 50 mg of complex powder. Taking aliquots at different time intervals, the UV-visible absorbance in time after rapid centrifugation was measured. Formula (1) was applied to calculate the dye adsorption efficiency.

$$H = [(C_0 - C)/C_0] \times 100\% \quad (1)$$

In the formula, η is the adsorption efficiency and C_0 is the concentration before adsorption, mg/L; C is the concentration after adsorption, mg/L.

3 RESULTS AND DISCUSSION

3.1 Description of the crystal structures

Single-crystal X-ray diffraction analysis reveals that each asymmetric unit contains a $[\text{LnL}_4(\text{H}_2\text{O})]^{3+}$, a $[\text{PMo}_{12}\text{O}_{40}]^{3-}$ and a acetonitrile molecule. Complexes **1**~**3** crystallize in the monoclinic system with space group $P2_1/c$. They are all

seven-coordinated by six oxygen atoms from three L ligands and one oxygen atom from a water molecule (Fig. 1). $[\text{PMo}_{12}\text{O}_{40}]^{3-}$ exists only as an anion. It is not involved in coordination, and remains unchanged in structure. Herein, we discuss complex **1** deeply to demonstrate the general structural features. In **1**, the Dy-O (P=O) bond lengths range from 2.261(12) to 2.300(11) Å. Compared with the similar complex $[\text{DyL}_2(\text{H}_2\text{O})_4]\text{Cl}_3 \cdot 6\text{H}_2\text{O}$ (L = tetrakis(O-isopropyl)methylenediphosphonate)^[17], the average distance of Dy-O (P=O) bonds (2.299 Å) in complex **1** is shorter and the (P)O-Dy-O(P) bond angle (77.0°) is slightly increased. The coordination spheres of three crystals are all composed of Ln-O bonds but with different lengths. Detailed information about other complexes was put in ESI. By analyzing different complexes, it found that the Ln-O bond lengths depend on the radii of rare earth ions ($r\text{Lu}^{3+}(0.861 \text{ Å}) < r\text{Ho}^{3+}(0.901 \text{ Å}) < r\text{Dy}^{3+}(0.912 \text{ Å})$). The bond lengths of Ln-O increase as the radius of metal grows in the order of Dy-O > Ho-O > Lu-O (Table 2). At the same time, the comparison of average (P)O-Ln-O(P) bond angle formed by L ligands chelation results in the following order: complex **3** > complex **2** > complex **1**.

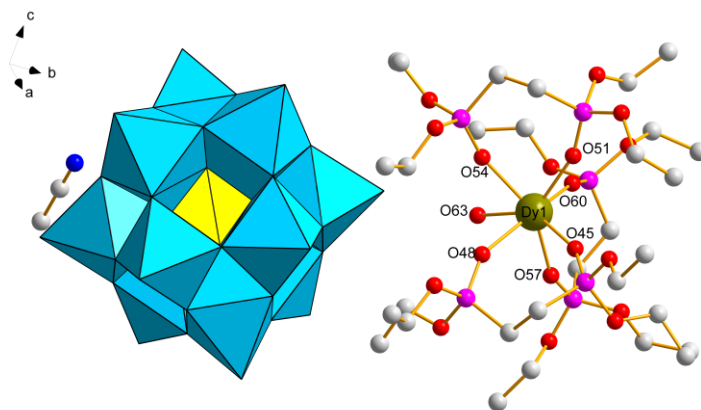


Fig. 1. Molecular structure of complex 1. Hydrogen atoms were omitted for clarity

Complex **1** forms a three-dimensional structure through the action of abundant hydrogen bonds (Fig. 2). Wherein the hydrogen bonds are mainly C–H···O constructed by the hydrogen atoms from L ligands and oxygen atoms from $[\text{PMo}_{12}\text{O}_{40}]^{3-}$. Interestingly, despite all complexes have similar structures, the number of hydrogen bonds is different. In a basic unit, the number of hydrogen bonds in complexes **1**~**3** is 10, 9, and 11, respectively. Moreover, the angles and

positions of hydrogen bonds vary with different complexes (Table 3). For **1**, the nitrogen atom from the acetonitrile combines with the O–H group from coordination water to form hydrogen bonds $\text{O}(63)\text{--H}(63\text{D})\cdots\text{N}(1)$. But in complexes **2** and **3**, the C–H groups come from acetonitrile and the oxygen atoms from $[\text{PMo}_{12}\text{O}_{40}]^{3-}$, resulting in hydrogen bonds like $\text{C}(32)\text{--H}(32\text{C})\cdots\text{O}(19)$ and $\text{C}(15)\text{--H}(15\text{A})\cdots\text{O}(8)$.

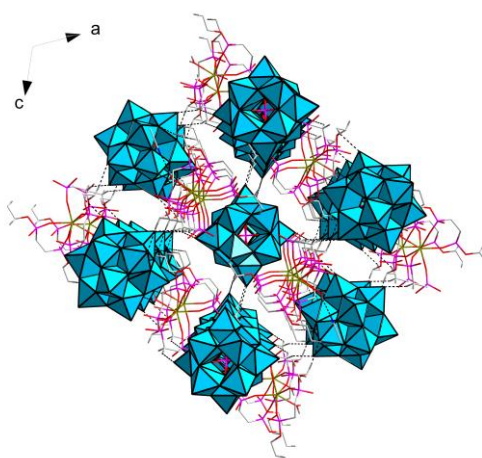


Fig. 2. Three-dimensional stacking structure of complex 1. Hydrogen atoms and carbon chains not related to hydrogen bonding were omitted for clarity

3.2 IR, PXRD and TG curves of complexes

The IR absorption spectra of complexes **1**~**3** were determined in the scope of 4000 to 400 cm^{-1} . Complexes **1**~**3** have very similar IR spectra, so only complex **1** is described in detail. For L ligands, the characteristic absorption band of $\nu(\text{C--P--O})$ at 1035 cm^{-1} shifts to 1034 cm^{-1} and that of $\nu(\text{P=O})$ at 1260 shifts to 1211 cm^{-1} ^[28]. All changes on the infrared absorption spectra are mainly caused by the coordination between P=O groups and rare earth ions. Besides, the bands at

$958\sim 803\text{ cm}^{-1}$ are attributed to the Mo–O–Mo and Mo=O characteristic bands from POM^[29].

Powder X-ray diffraction of complexes **1**~**3** shows that the samples have obvious crystal phase diffraction peaks in the range of $5\sim 50^\circ$. The main peaks of the synthesized samples in the spectra are consistent well with the simulation results, indicating the high crystal phase purity of powder samples complexes **1**~**3** (Fig. 3).

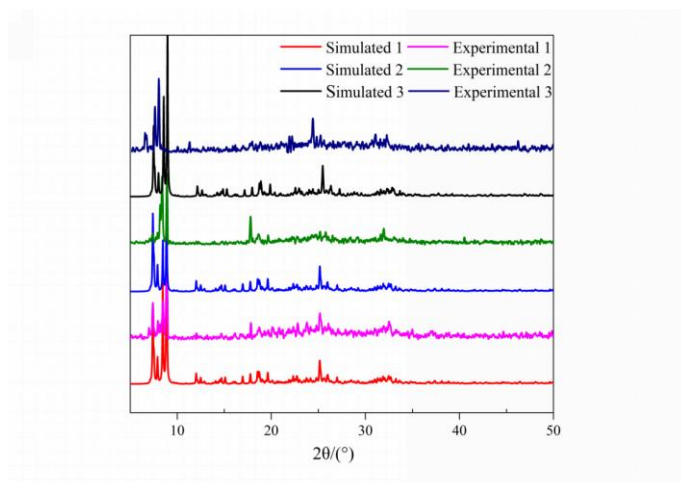


Fig. 3. Powder PXRD patterns of complexes 1~3 compared with the simulation results

The thermal stability characterization of complexes **1**~**3** was carried out in nitrogen atmosphere from 30 to 850 °C at an average heating rate of 10 °C/min. As shown in Fig. 4, the TG curves for complexes **1**~**3** display initial weight loss of 1.7% (calcd. 2.0%) for **1**, 2.6% (calcd. 2.0%) for **2** and 3.2%

(calcd. 2.0%) for **3** in the 30~240 °C region, which can be attributed to the loss of acetonitrile in crystal lattice and one coordinated water molecule. Then the dehydrated complexes **1**~**3** begin to decompose at 240 °C and the TG curve shows a maximum mass loss rate at 240~370 °C.

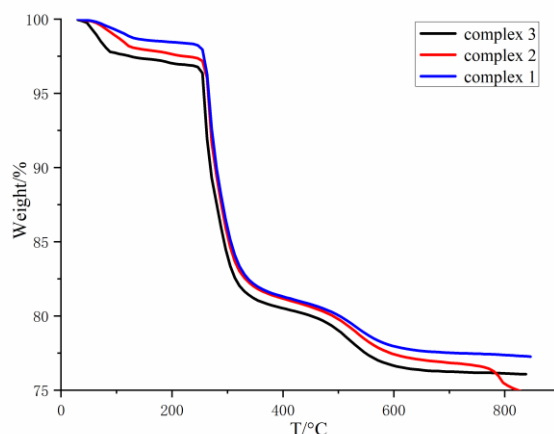


Fig. 4. TG curves of complexes 1~3

3.3 Adsorption of dyes by complexes

Adsorption is a simple and effective method during purification process of dye wastewater. Based on electrostatic interaction, RhB, as a cationic dye, can be effectively handled by large volume of $[\text{PMo}_{12}\text{O}_{40}]^{3-}$ added to the complexes. During the adsorption experiment, 1.5 mL of sample solution was collected at certain intervals, and UV-vis spectroscopy was performed after centrifugation at 10000 r/min. The results show that complexes **1**~**3** have excellent dye adsorption performance and RhB was adsorbed significantly within 5

minutes (Fig. 5). It is worth noting that among the three complexes, **1** has the highest adsorption efficiency with the rate being 92.22% at 5 minutes, and reaching 93.54% after 30 minutes. In order to confirm that only adsorption but no degradation occurs, the samples after adsorption were soaked in ethanol, and the existence of RhB was proved by UV-vis spectroscopy. We also monitored the PXRD patterns after adsorption and desorption, indicating that the framework of **1** is stable and maintains during the processes.

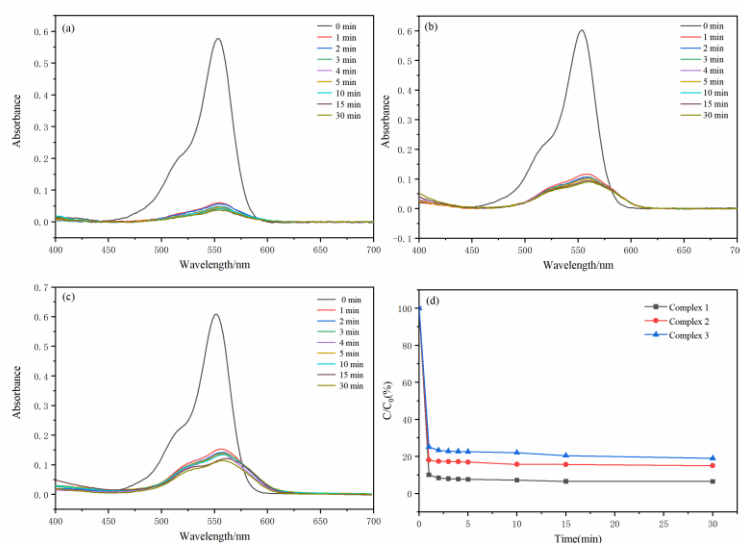


Fig. 5. (a)-(c) UV-Vis spectra of RhB solutions under different adsorption time: (a) complex 1; (b) complex 2; (c) complex 3. (d) Adsorption efficiency of RhB by complexes 1~3

The effects of the different initial concentration on the adsorption of RhB for complex 1 are shown in Fig. 6. It is obvious that the adsorption capacity increased gradually from 35.95 to 113.93 mg/g with the increase of the initial concentration of RhB. Moreover, there was little increase for the adsorption capacity corresponding to the initial concentra-

tion of RhB from 180 to 200 mg/L, which indicated that a saturated adsorption capacity has been attained. The adsorption capacity of complex 1 is better than that of the ordinary adsorbents such as Sago waste derived activated carbon, 16.1 mg/g^[30] and acid-functionalized multiwalled carbon nanotubes, 42.68 mg/g^[31].

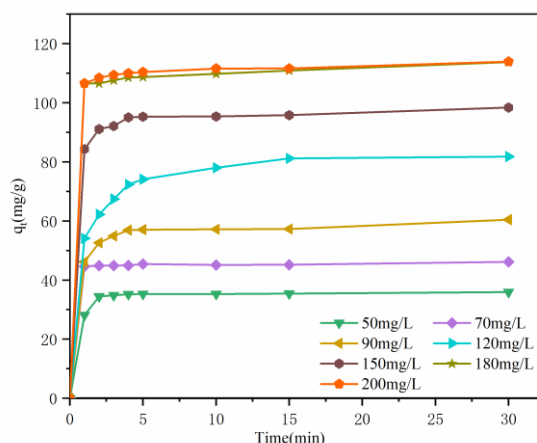


Fig. 6. Effects of initial concentration on the adsorption of RhB in complex 1

The three complexes have similar structures but different intermolecular interactions, leading to a small gap in their adsorption performance. It is speculated that the slight difference can be attributed to the difference in hydrogen bonds between molecules, especially the hydrogen bonds on

the surface of $[\text{PMo}_{12}\text{O}_{40}]^{3-}$, which may affect the diffusion of dye molecules.

3.4 Terahertz time domain spectroscopy (THz-TDS)

The terahertz time-domain spectroscopy (THz-TDS) of $\text{H}_3\text{PMo}_{12}\text{O}_{40} \cdot n\text{H}_2\text{O}$ and complexes 1~3 were measured in the

range of 0.2~2.8 THz at room temperature. All the above compounds have characteristic resonance peaks, which may be explained by the factors of polar molecules and dipoles rotating and vibrating, resulting in strong absorption and chromatic dispersion. The peaks found for them are as follows: $\text{H}_3\text{PMo}_{12}\text{O}_{40} \cdot n\text{H}_2\text{O}$ (0.38, 0.53, 0.64, 0.73, 1.84, 1.96, 2.13, 2.22, 2.31, 2.40, 2.46, 2.55, 2.66, 2.75 THz) (Fig. 7); L ligand (0.90, 1.05, 1.20, 1.25, 1.46, 1.55, 1.76, 1.90, 2.10, 2.10, 2.31, 2.51, 2.57, 2.72 THz) (Fig. 8); complex **1** (0.32, 0.38, 0.44, 0.56, 0.64, 0.82, 0.91, 1.05, 1.20, 1.28, 1.37, 1.46, 1.55, 1.84, 1.99, 2.10, 2.19, 2.28, 2.37, 2.45, 2.52, 2.72 THz); complex **2** (0.32, 0.38, 0.44, 0.56, 0.70, 0.82, 0.93, 1.05, 1.20, 1.28, 1.37, 1.46, 1.55, 1.84, 1.90, 1.99, 2.04, 2.19, 2.31, 2.45, 2.52, 2.60, 2.72 THz) and complex **3** (0.38, 0.44, 0.53, 0.64, 0.73, 0.82, 0.91, 0.99, 1.20, 1.25, 1.37, 1.46, 1.55, 1.75, 1.84, 1.90, 1.99, 2.10, 2.19, 2.31, 2.44, 2.52, 2.60, 2.66, 2.75 THz) (Fig. 9). The THz absorption spectra of $\text{H}_3\text{PMo}_{12}\text{O}_{40} \cdot n\text{H}_2\text{O}$ show a rising trend in the range of 0.2~2.8 THz and have many obvious peaks in the range of 1.84~2.75 THz. The THz absorption spectra of L ligand show the first rise and fall, and have a lot of tiny peaks in the 0.9~2.8 THz region.

Complexes **1**~**3** have almost consistent THz absorption spectra due to their similar structures. By comparing the THz absorption spectra of the products with L ligand and $\text{H}_3\text{PMo}_{12}\text{O}_{40} \cdot n\text{H}_2\text{O}$, we can easily find that some peaks of the reactants disappear or move in the complexes, which can be attributed to the generation of new structures and intermolecular interactions. The peak shapes of complexes **1**~**3** in 1.84~2.75 THz were different, which is likely to reflect the difference in the weak intermolecular forces that cause the different adsorption efficiency. Because of many hydrogen bonds in complexes, it is not easy to make tentative assignments of peaks in the terahertz region for the samples. However, it is worth noting that the construction of hydrogen bonds in complex **1** is different from that of complexes **2** and **3**, so the peak of **1** at 1.75 THz may correspond to its unique hydrogen bond of $\text{O}-\text{H} \cdots \text{N}^{[32]}$. The relationship between terahertz spectroscopy and the structure and properties of the complex needs further exploration. The results in this paper act as a supplement to the THz spectroscopic properties of lanthanide complexes containing phosphorous ligand.

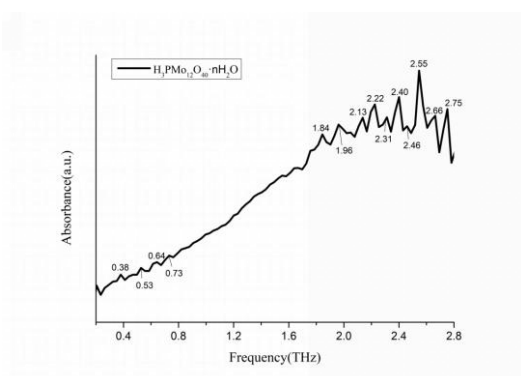


Fig. 7. Terahertz spectrum of $\text{H}_3\text{PMo}_{12}\text{O}_{40} \cdot n\text{H}_2\text{O}$ in the range of 0.2~2.8 THz

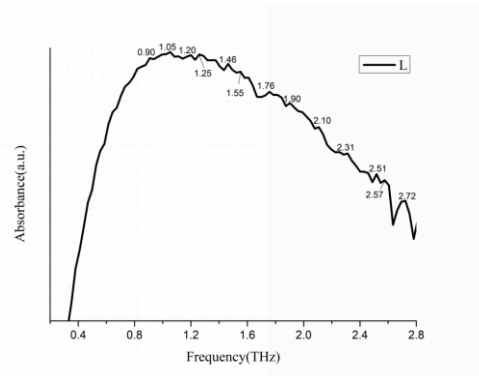


Fig. 8. Terahertz spectrum of tetraethyl ethylenediphosphonate in the range of 0.2~2.8 THz

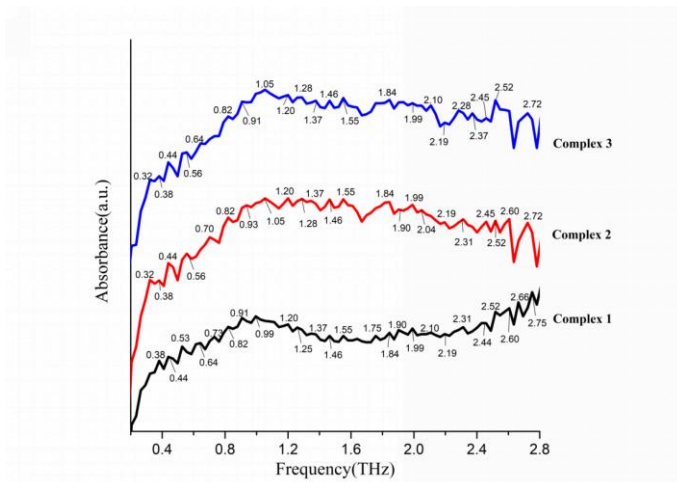


Fig. 9. Terahertz spectra of complexes **1**~**3** in the range 0.2~2.8 THz

4 CONCLUSION

Three novel Ln(III) complexes, namely $[\text{DyL}_3(\text{H}_2\text{O})]\text{PMo}_{12}\text{O}_{40}\text{CH}_3\text{CN}$ (**1**), $[\text{HoL}_3(\text{H}_2\text{O})]\text{PMo}_{12}\text{O}_{40}\text{CH}_3\text{CN}$ (**2**) and $[\text{LuL}_3(\text{H}_2\text{O})]\text{PMo}_{12}\text{O}_{40}\text{CH}_3\text{CN}$ (**3**), have been synthesized and characterized by single-crystal X-ray diffraction, elemental analysis, PXRD, thermogravimetric analysis and THz time-domain spectroscopy (THz-TDS). All complexes are seven-coordinated mononuclear structures and the unit cells pack into a 3D structure by hydrogen bonds. PXRD and

TG curves show good sample purity and thermal stability of the samples. Complex **1** has the highest adsorption performance for rhodamine B. Terahertz spectroscopy was used for the first time to characterize lanthanide phosphonate complexes based on $[\text{PMo}_{12}\text{O}_{40}]^{3-}$ modified. The peak of complex **1** at 1.75 terahertz is related to hydrogen bond of $\text{O}-\text{H}\cdots\text{N}$. Terahertz time-domain spectroscopy can act as a characterization method to analyze the changes of absorption peaks caused by intermolecular forces, which provide a spectroscopic basis for the rapid detection of weak intermolecular forces in complexes.

REFERENCES

- (1) Hasegawa, Y.; Kitagawa, Y. Thermo-sensitive luminescence of lanthanide complexes, clusters, coordination polymers and metal-organic frameworks with organic photosensitizers. *J. Mater. Chem. C* **2019**, 7, 7494–7511.
- (2) Wen, H. R.; Hu, J. J.; Yang, K.; Zhang, J. L.; Liu, S. J.; Liao, J. S.; Liu, C. M. Family of chiral $\text{Zn}^{\text{II}}\text{-Ln}^{\text{III}}$ (Ln = Dy and Tb heterometallic complexes derived from the amine-phenol ligand showing multifunctional properties. *Inorg. Chem.* **2020**, 59, 2811–2824.
- (3) Kariaka, N. S.; Trush, V. A.; Smola, S. S.; Fadiev, Y. M.; Dyakonenco, V. V.; Shishkina, S. V.; Sliva, T. Y.; Amirkhanov, V. M. Highly luminescent diphenyl-N-benzoylamidophosphate based lanthanide tetrakis-complexes. *J. Lumin.* **2018**, 194, 108–115.
- (4) Lyubov, D. M.; Tolpygin, A. O.; Trifonov, A. A. Rare-earth metal complexes as catalysts for ring-opening polymerization of cyclic esters. *Coord. Chem. Rev.* **2019**, 83–145.
- (5) Li, M.; Wang, C.; Chen, J.; Guo, Z.; Mou, Z.; Luo, Y. Controlled iso-specific polymerization of 2-vinylpyridine catalyzed by arylamide-ligated rare-earth metal aminobenzyl complexes. *Dalton Trans.* **2018**, 47, 15967–15976.
- (6) Hua, L. Y.; Li, B. X.; Han, C. T.; Gao, P. F.; Wang, Y. R.; Yuan, D.; Yao, Y. M. Synthesis of homo- and heteronuclear rare-earth metal complexes stabilized by ethanolamine-bridged bis(phenolato) ligands and their application in catalyzing reactions of CO_2 and epoxides. *Inorg. Chem.* **2019**, 58, 8755–8786.
- (7) Jia, J. H.; Li, Q. W.; Chen, Y. C.; Liu, J. L.; Tong, M. L. Luminescent single-molecule magnets based on lanthanides: design strategies, recent advances and magneto-luminescent studies. *Coord. Chem. Rev.* **2019**, 378, 365–381.
- (8) Meihaus, K. R.; Fieser, M. E.; Corbey, J. F.; Evans, W. J.; Long, J. R. Record high single-ion magnetic moments through 4f_n5d₁ electron configurations in the divalent lanthanide complexes $[(\text{C}_5\text{H}_4\text{SiMe}_3)_3\text{Ln}]^+$. *J. Am. Chem. Soc.* **2015**, 9855–9860.
- (9) Latendresse, T. P.; Vieru, V.; Wilkins, B. O.; Bhuvanesh, N. S.; Chibotaru, L. F.; Nippe, M. Magnetic properties of a terbium-[1]ferrocenophane complex: analogies between lanthanide-ferrocenophane and lanthanide-bis-phthalocyanine complexes. *Angew. Chem. Int. Edit.* **2018**, 57, 8164–8169.
- (10) Platt, A. W. G. Lanthanide phosphine oxide complexes. *Coord. Chem. Rev.* **2017**, 340, 62–78.
- (11) Matveeva, A. G.; Vologzhanina, A. V.; Goryunov, E. I.; Aysin, R. R.; Pasechnik, M. P.; Matveev, S. V.; Godovikov, I. A.; Safiulina, A. M.; Brel, V. K. Extraction and coordination studies of a carbonyl-phosphine oxide scorpionate ligand with uranyl and lanthanide(III) nitrates: structural, spectroscopic and DFT characterization of the complexes. *Dalton Trans.* **2016**, 45, 5162–5179.
- (12) Maxim, C.; Branzea, D. G.; Tiseanu, C.; Rouzies, M.; Clerac, R.; Andruh, M.; Avarvari, N. Cyanomethylene-bis(phosphonate)-based lanthanide complexes: structural, photophysical, and magnetic investigations. *Inorg. Chem.* **2014**, 53, 2708–2717.
- (13) Tang, X. Y.; Hua, J. K.; Ma, Y. S.; Hori, A.; Yuan, R. X.; Matsuda, R. Tetrametallic Ln(III) (Ln = Gd, Dy) phosphonate clusters: spin cooler and single-molecule magnet. *Inorg. Chim. Acta* **2018**, 482, 900–904.
- (14) Glasneck, F.; Kobalz, K.; Kersting, B. Lanthanide complexes of a calix[4]arene ligand with dangling phosphonate and picolinamide arms: synthesis, crystal structures, and extraction properties. *Eur. J. Inorg. Chem.* **2016**, 3111–3122.
- (15) Du, D. Y.; Yan, L. K.; Su, Z. M.; Li, S. L.; Lan, Y. Q.; Wang, E. B. Chiral polyoxometalate-based materials: from design syntheses to functional applications. *Coord. Chem. Rev.* **2013**, 257, 702–717.
- (16) Wang, Y. F.; Weinstock, I. A. Polyoxometalate-decorated nanoparticles. *Chem. Soc. Rev.* **2012**, 41, 7479–7496.

- (17) Proust, A.; Matt, B.; Villanneau, R.; Guillemot, G.; Gouzerh, P.; Izzet, G. Functionalization and post-functionalization: a step towards polyoxometalate-based materials. *Chem. Soc. Rev.* **2012**, 41, 7605–7622.
- (18) Wei, M. L.; He, C.; Hua, W.; Duan, C.; Li, S.; Meng, Q. J. A large protonated water cluster $H^+(H_2O)_{27}$ in a three-dimensional metal-organic framework. *J. Am. Chem. Soc.* **2006**, 128, 13318–13319.
- (19) Han, Q. X.; He, C.; Zhao, M.; Qi, B.; Niu, J. Y.; Duan, C. Y. Engineering chiral polyoxometalate hybrid metal-organic frameworks for asymmetric dihydroxylation of olefins. *J. Am. Chem. Soc.* **2013**, 135, 10186–10189.
- (20) McIntosh, A. I.; Yang, B.; Goldup, S. M.; Watkinson, M.; Donnan, R. S. Terahertz spectroscopy: a powerful new tool for the chemical sciences? *Chem. Soc. Rev.* **2012**, 41, 2072–2082.
- (21) Shi, L.; Duan, X. H.; Zhu, L. G.; Liu, X.; Pei, C. H. Directly insight into the inter- and intramolecular interactions of CL-20/TNT energetic cocrystal through the theoretical simulations of THz spectroscopy. *J. Phys. Chem. A* **2016**, 120, 1160–1167.
- (22) Sun, L. Z.; Wang, Y.; Lin, S.; Liu, J. M.; Li, Z. F.; Zhang, J. W.; Jin, Q. H. Synthesis, characterization and luminescent properties of two copper(I) complexes based on 2,2'-biquinoline and phosphorous ligand. *Chin. J. Struct. Chem.* **2018**, 37, 1313–1322.
- (23) Xu, S.; Liu, M.; Yang, Y. P.; Jiang, Y. H.; Li, Z. F.; Jin, Q. H.; Wang, X.; Xue, X. N. Syntheses, structures, luminescence, NMR spectra and terahertz time-domain spectroscopy of nine lanthanide triflate complexes of tetrakis(*O*-isopropyl)methylenedisphosphonate with a L:Ln ratio of 4:1. *Polyhedron* **2015**, 87, 293–301.
- (24) Yang, Y. S.; Liu, M.; Yang, Y. P.; Jin, Q. H.; Li, Z. F.; Xue, X. N.; Zhang, Z. J.; Zheng, W. J. Synthesis, structures, luminescence and terahertz time-domain spectroscopy of seven lanthanide complexes with tetrakis(*O*-isopropyl)methylenedisphosphonate and 1,10-phenanthroline. *Polyhedron* **2015**, 93, 66–75.
- (25) Ma, Y.; Yang, Y. S.; Jiang, Y. H.; Li, Y. X.; Liu, M.; Li, Z. F.; Han, H. L.; Yang, Y. P.; Xin, X. L.; Jin, Q. H. Lanthanide contraction and chelating effect on a new family of lanthanide complexes with tetrakis(*O*-isopropyl)methylenedisphosphonate: synthesis, structures and terahertz time-domain spectroscopy. *RSC Adv.* **2017**, 7, 41651–41666.
- (26) Sheldrick, G. M. *SHELXS-97 and SHELXL-97, Software for Crystal Structure Analysis*. Siemens Analytical X-ray Instruments Inc., Madison, WI, USA **1997**.
- (27) Sheldrick, G. M. *SHELXTL NT Version 5.1, Program for Solution and Refinement of Crystal Structures*. University of Gottingen, Germany **1997**.
- (28) Hashimoto, M.; Koyano, G.; Mizuno, N. *In situ* IR spectrum of 12-tungstophosphoric acid hexahydrate with planar $H_3O_2^+$. *J. Phys. Chem. B* **2004**, 108, 12368–12374.
- (29) Haupt, E. T. K.; Kopf, J.; Petrova, J.; Arabadzhiev, V.; Momchilova, S. Complexes of esters of ethylenedisphosphonic acid with lanthanide nitrates: synthesis and structure. *Heteroatom Chem.* **2005**, 17, 36–46.
- (30) Kadirvelu, K.; Karthika, C.; Vennilamani, N.; Pattabhi, S. Activated carbon from industrial solid waste as an adsorbent for the removal of rhodamine-B from aqueous solution: kinetic and equilibrium studies. *Chemosphere* **2005**, 60, 1009–1017.
- (31) Oyetade, O. A.; Nyamori, V. O.; Martincigh, B. S.; Jonnalagadda, S. B. Effectiveness of carbon nanotube-cobalt ferrite nanocomposites for the adsorption of rhodamine B from aqueous solutions. *RSC Adv.* **2015**, 5, 22724–22739.
- (32) Nguyen, K. L.; Friscic, T.; Day, G. M.; Gladden, L. F.; Jones, W. Terahertz time-domain spectroscopy and the quantitative monitoring of mechanochemical cocrystal formation. *Nat. Mater.* **2007**, 6, 206–209.